JCTC Journal of Chemical Theory and Computation

pubs.acs.org/JCTC Article

Accurate Boundary Integral Formulations for the Calculation of Electrostatic Forces with an Implicit-Solvent Model

Ian Addison-Smith, Horacio V. Guzman, and Christopher D. Cooper*

Cite This: J. Chem. Theory Comput. 2023, 19, 2996−3006

Read Online

ACCESS | Metrics & More | Article Recommendations

ABSTRACT: An accurate force calculation with the Poisson−Boltzmann equation is challenging, as it requires the electric field on the molecular surface. Here we present a calculation of the electric field on the solute−solvent interface that is exact for piecewise linear variations of the potential and analyze four different alternatives to compute the force using a boundary element method. We performed a verification exercise for two cases: the isolated and two interacting molecules. Our results suggest that the boundary element method outperforms the finite difference method, as the latter needs a much finer mesh than in solvation energy calculations to get acceptable accuracy in the force, whereas the same surface mesh as in a standard energy calculation is appropriate for the boundary element method. Among the four evaluated alternatives of force calculation, we saw that the most accurate one is based on the Maxwell stress tensor. However, for a realistic application, like the barnase−barstar complex, the approach based on variations of the energy functional, which is less accurate, gives equivalent results. This analysis is useful toward using the Poisson−Boltzmann equation for force calculations in applications where high accuracy is key, for example, to feed molecular dynamics models or to enable the study of the interaction between large molecular structures, like viruses adsorbed onto substrates.

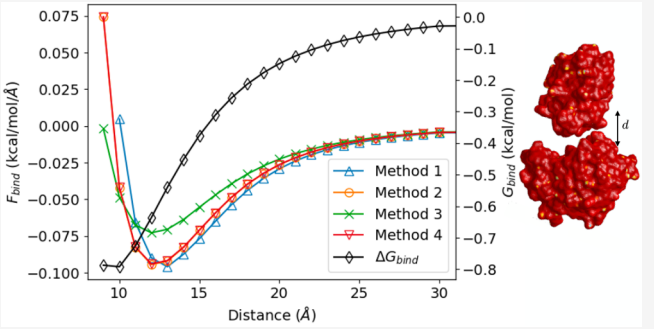

INTRODUCTION

Implicit-solvent models consider a dissolved molecule as a cavity inside an infinite dielectric medium, averaging out the discrete degrees of freedom of the solvent,[1,2] which yields an efficient way to compute mean-field potentials and free energies. A popular version of these models uses the Poisson−Boltzmann equation to represent the electrostatic potential in an ionic solvent.[3] Numerical solutions of this equation are implemented in a variety of solvers that use finite difference,[4−6] finite element,[4,7] or boundary element (BEM) methods.[8−11]

Most applications of the Poisson−Boltzmann model apply it to compute the mean-field electrostatic potential and polar component of the solvation energy, but it can also compute the electrostatic force.[4,5,12−14] This force is useful to study the interaction between multiple bodies,[15] which can be fed into molecular dynamics codes (i.e., for molecular docking[12]).

There are three ways to compute the force with the Poisson−Boltzmann equation: starting from the variation of the energy functional,[9,16−18] using the Maxwell stress tensor,[19,20] or calculating the variation of the solvation energy numerically.[18] Regardless of the method of choice, this calculation is challenging, as it involves either (*i*) the subtraction of two large numbers,[16] (*ii*) calculating hypersingular integrals,[19] or (*iii*) numerical differentiation across the molecular surface.[21] It is also model-dependent, as there are differences if the dielectric interface is sharp or continuous.[22] Moreover, if the Poisson−Boltzmann equation is being solved with a finite difference method, the electric field on the molecular surface is computed with a mollified interface[5,12] or approximated with least-squares,[23] which may introduce a diffusive effect to the solution. The boundary element method offers a more accurate description of the molecular surface, but current implementations do not overcome the limitations described earlier.[24] Alternatively, we can reformulate the expressions resulting from taking the variation of the energy functional and the Maxwell stress tensor in terms of an apparent surface charge.[20,25,26] Also, analytical calculations of the force are possible when using the conductor-like screening model (COSMO)-type models.[14]

The goal of this work is twofold. First, we present a new formulation to compute the electric field across the boundary

Received: January 5, 2023
Published: April 27, 2023

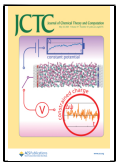

https://doi.org/10.1021/acs.jctc.3c00021
J. Chem. Theory Comput. 2023, 19, 2996−3006

that is exact for piecewise linear boundary elements. This allows us to compute the force without adding numerical approximations on top of standard electrostatic potential calculations. Second, we perform a thorough assessment of the accuracy of the force computed with different methods, implemented in the Poisson−Boltzmann & Jupyter (PBJ) code.[27]

In Methods we present the implicit-solvent model and how the Poisson−Boltzmann equation is formulated with a boundary integral approach. This section also gives details on the calculation of the energy and force in a Poisson−Boltzmann continuum. In the Results and Discussion we show the accuracy of the different methods for the force calculation in settings with isolated and interacting molecules. The final section presents conclusions and outlook for future work.

METHODS

The Poisson−Boltzmann Equation with a Boundary Integral Formulation. In the context of molecular solvation, the Poisson−Boltzmann model considers the solute as a low-dielectric cavity immersed in an infinite continuum domain. Following Figure 1, the *solute* region (Ω_1) has point sources to represent the partial charges (q_k) and is contained inside the molecular surface (Γ). There are several possible definitions of Γ, such as the solvent-accessible, solvent-excluded, van der Waals, and Gaussian surfaces. We chose the solvent-excluded surface,[28] which is the result of tracking the contact points between the solute and a spherical probe that is rolled around it. On the other hand, the external region corresponds to an ionic solvent (usually, water with salt). The free ions in the solvent have an effect on the electric field, and if they are considered as point charges that arrange according to Boltzmann statistics, continuum electrostatic theory leads to the (linearized) Poisson−Boltzmann equation. We can express this as the following system of partial differential equations:

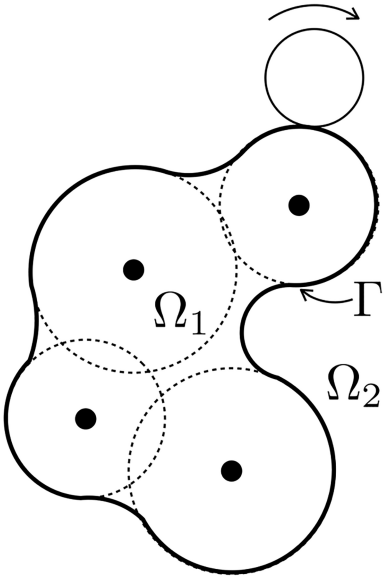

Figure 1. Representation of a solute in a continuum model.

$$\begin{aligned} \nabla^2\phi_1 &= \frac{1}{\epsilon_1}\sum_{k=1}^{N_q} q_k\delta(\mathbf{x}_k) && \mathbf{x}\in\Omega_1 \\ (\nabla^2-\kappa^2)\phi_2 &= 0 && \mathbf{x}\in\Omega_2 \\ \phi_1 &= \phi_2;\quad \epsilon_1\frac{\partial\phi_1}{\partial\mathbf{n}} = \epsilon_2\frac{\partial\phi_2}{\partial\mathbf{n}} && \mathbf{x}\in\Gamma \end{aligned} \tag{1}$$

where ϕ is the electric potential, κ is the inverse of the Debye length, $\delta(\mathbf{x}_k)$ is the Dirac delta function at $\mathbf{x}_k$, and $\mathbf{n}$ is a unit vector that is normal to Γ.

The Boundary Integral Formulation. A common approach is to formulate eq 1 as an integral over Γ. Applying Green's second identity to eq 1, we arrive at

$$\begin{aligned} \phi_1(\mathbf{x}) &= -K^{\mathbf{x}}_{\Gamma,\mathrm{L}}(\phi_{1,\Gamma}) + V^{\mathbf{x}}_{\Gamma,\mathrm{L}}\left(\frac{\partial\phi_{1,\Gamma}}{\partial\mathbf{n}}\right) \\ &\quad + \frac{1}{\epsilon_1}\sum_{k=1}^{N_q}\frac{q_k}{4\pi|\mathbf{x}-\mathbf{x}_k|}, \qquad \mathbf{x}\in\Omega_1 \\ \phi_2(\mathbf{x}) &= K^{\mathbf{x}}_{\Gamma,\mathrm{Y}}(\phi_{2,\Gamma}) - V^{\mathbf{x}}_{\Gamma,\mathrm{Y}}\left(\frac{\partial\phi_{2,\Gamma}}{\partial\mathbf{n}}\right), \qquad \mathbf{x}\in\Omega_2 \end{aligned} \tag{2}$$

where $\mathbf{x}\in\Omega_1\cup\Omega_2\backslash\Gamma$. Also,

$$\begin{aligned} V^{\mathbf{x}}_{\Gamma}(\varphi) &= \oint_{\Gamma} G(\mathbf{x},\mathbf{x}')\varphi(\mathbf{x}')\,\mathrm{d}\mathbf{x}' \\ K^{\mathbf{x}}_{\Gamma}(\varphi) &= \oint_{\Gamma}\frac{\partial G}{\partial\mathbf{n}}(\mathbf{x},\mathbf{x}')\varphi(\mathbf{x}')\,\mathrm{d}\mathbf{x}' \end{aligned} \tag{3}$$

are known as the single- and double-layer potentials, and

$$\begin{aligned} G_{\mathrm{L}}(\mathbf{x},\mathbf{x}') &= \frac{1}{4\pi|\mathbf{x}-\mathbf{x}'|} \\ G_{\mathrm{Y}}(\mathbf{x},\mathbf{x}') &= \frac{\mathrm{e}^{-\kappa|\mathbf{x}-\mathbf{x}'|}}{4\pi|\mathbf{x}-\mathbf{x}'|} \end{aligned} \tag{4}$$

are the free-space Green's functions of the Laplace and Yukawa (Poisson−Boltzmann) potentials.

Combinations of the expressions in eq 2 yield different boundary integral formulations[27] that vary in complexity and the conditioning of the resulting matrix. Here we use the simplest form, termed *direct formulation*,[29] which is implemented in the PBJ code.[27] The direct formulation simply takes the limit of the expressions in eq 2 as $\mathbf{x}\to\Gamma$, leaving

$$\begin{aligned} \frac{\phi_{1,\Gamma}}{2} + K^{\Gamma}_{\Gamma,\mathrm{L}}(\phi_{1,\Gamma}) - V^{\Gamma}_{\Gamma,\mathrm{L}}\left(\frac{\partial\phi_{1,\Gamma}}{\partial\mathbf{n}}\right) &= \frac{1}{\epsilon_1}\sum_{k=1}^{N_q}\frac{q_k}{4\pi|\mathbf{x}_\Gamma-\mathbf{x}_k|} \\ \frac{\phi_{1,\Gamma}}{2} - K^{\Gamma}_{\Gamma,\mathrm{Y}}(\phi_{1,\Gamma}) + \frac{\epsilon_1}{\epsilon_2}V^{\Gamma}_{\Gamma,\mathrm{Y}}\left(\frac{\partial\phi_{1,\Gamma}}{\partial\mathbf{n}}\right) &= 0 \end{aligned} \tag{5}$$

There are many other boundary integral formulations of this problem[27] that yield better-conditioned systems than eq 5, for example, Juffer's[30] and Lu's[31] formulations. The force calculation presented in this work is applicable to any formulation.

Energy in a Poisson−Boltzmann Continuum. In a continuum description, the electrostatic free energy is a function of the electrostatic potential (ϕ), the charge distribution in the solute $\left(\rho_{\mathrm{f}} = \sum_{j=1}^{N_q} q_j\delta(\mathbf{x}_j)\right)$, and the

https://doi.org/10.1021/acs.jctc.3c00021
J. Chem. Theory Comput. 2023, 19, 2996−3006

concentration of free ions in the solvent (c_j for species j). At equilibrium, c_j takes the Boltzmann distribution. This transforms Gauss's law into the Poisson−Boltzmann equation, and the Gibbs free energy functional takes the form[32]

$$G = \int_\Omega \left[\rho_f \phi - \frac{\epsilon(\mathbf{x})}{2} |\nabla\phi|^2 - \beta^{-1} \sum_{j=1}^{M} c_j^\infty (e^{-\beta q_j \phi} - 1)\lambda \right] d\mathbf{x} \tag{6}$$

where $\beta = 1/kT$ is the inverse thermal energy, c_j^∞ is the bulk concentration far away from the solute at vanishing electrostatic potential, and λ is a unit-step function that masks out the salt-free solute region. In linear form, eq 6 becomes[3]

$$G = \int_\Omega \left[\rho_f \phi - \frac{\epsilon(\mathbf{x})}{2} |\nabla\phi|^2 - \frac{1}{2}\epsilon(\mathbf{x})\kappa^2\phi^2\lambda \right] d\mathbf{x} \tag{7}$$

At equilibrium, the free energy G reaches a minimum value.[32] Using the Euler−Lagrange equation, the minimum is

$$\begin{aligned} &\frac{\partial G}{\partial \phi} - \sum_{j=1}^{n} \frac{\partial}{\partial x_j}\left(\frac{\partial G}{\partial \phi_{x_j}}\right) = 0 \\ &\Rightarrow \rho_f - \epsilon(\mathbf{x})\kappa^2\phi\lambda + \nabla\cdot(\epsilon(\mathbf{x})\nabla\phi) = 0 \\ &\Rightarrow \nabla\cdot(\epsilon(\mathbf{x})\nabla\phi) = -\rho_f + \epsilon(\mathbf{x})\kappa^2\phi\lambda \end{aligned} \tag{8}$$

where x_j ($j \in \{1, 2, 3\}$) are the components of $\mathbf{x}$. Equation 8 shows that the electrostatic potential that minimizes the energy is a solution of the Poisson−Boltzmann equation. We can use the identity $\nabla\cdot(\epsilon\phi\nabla\phi) = \phi\nabla\cdot(\epsilon\nabla\phi) + \epsilon\nabla\phi\cdot\nabla\phi$ and consider $\int_\Omega \nabla\cdot(\epsilon\phi\nabla\phi)\, d\Omega = 0$ (as ϕ goes to 0 at infinity) to rewrite eq 7 as

$$\begin{aligned} G &= \int_\Omega \left[\rho_f\phi + \frac{1}{2}(\phi\nabla\cdot(\epsilon(x)\nabla\phi)) - \frac{1}{2}\epsilon(\mathbf{x})\kappa^2\phi^2\lambda \right] d\mathbf{x} \\ &= \int_\Omega \left[\rho_f\phi + \frac{1}{2}\phi(-\rho_f + \epsilon(\mathbf{x})\kappa^2\phi\lambda)) - \frac{1}{2}\epsilon(\mathbf{x})\kappa^2\phi^2\lambda \right] d\mathbf{x} \\ &= \frac{1}{2}\int_\Omega \rho_f\phi\, d\mathbf{x} \end{aligned}$$

Acknowledging that the charge distribution in the solute is a set of Dirac delta functions and that the solvation process is the difference between vacuum and solvated states, we arrive at the well-known expression for solvation energy:

$$\Delta G_{solv} = \frac{1}{2}\sum_{k=1}^{N_q} q_k \phi_{reac}(\mathbf{x}_k) \tag{9}$$

where $\phi_{reac} = \phi - \phi_{Coul}$ is the reaction potential at the location of the atoms ($\mathbf{x}_k$). In the context of the boundary integral formulation, ϕ_{reac} can be computed by subtracting out the Coulomb contribution from the first expression in eq 2 as follows:

$$\phi_{reac}(\mathbf{x}) = -K_{\Gamma,L}^{\mathbf{x}}(\phi_{1,\Gamma}) + V_{\Gamma,L}^{\mathbf{x}}\left(\frac{\partial\phi_{1,\Gamma}}{\partial\mathbf{n}}\right) \tag{10}$$

Forces in a Poisson−Boltzmann Continuum. *Virtual Displacement Approach.* Force is the gradient of the energy in eq 7 along a coordinate. Thus, we can use the virtual work principle to compute the force by evaluating the energy at positions displaced by a small value h[18] and performing a finite-difference-type calculation:

$$F_i(\mathbf{x}) = -\frac{\partial G}{\partial x_i}(\mathbf{x}) \approx -\left(\frac{G(\mathbf{x} + h\mathbf{e}_i) - G(\mathbf{x} - h\mathbf{e}_i)}{2h}\right) \tag{11}$$

Here we can compute any component of the force by performing the displacements in the corresponding direction x, y, or z. This approach is convenient because it does not involve any modification of a standard Poisson−Boltzmann solver that can compute the energy. However, accuracy becomes an issue, as energy differences are usually small, and the numerical solver needs to appropriately resolve the electrostatic potential, requiring meshes that are much finer than in common solvation energy calculations. On top of this, it requires multiple energy calculations, increasing calculation time.

Energy Functional Variation Approach. Gilson et al.[16] used the virtual work principle to take variations of the energy functional in eq 7 to find a force density function. This is

$$\mathbf{f} = \rho_f\mathbf{E} - \frac{1}{2}|\mathbf{E}|^2\nabla\epsilon - \frac{1}{2}\epsilon\kappa^2\phi^2\nabla\lambda \tag{12}$$

which can be integrated in the volume to find the total force. We refer the reader to the work by Gilson et al.[16] for the complete derivation that leads to eq 12.

Equation 12 introduces a clear distinction between three sources of force:

- Charge, due to the electric field ($\mathbf{E}$) on the charges:

$$\mathbf{F}_q = \int_\Omega \rho_f\mathbf{E}\, d\mathbf{x} \tag{13}$$

  Similar to the electrostatic potential, $\mathbf{E}$ can be decomposed into Coulombic ($\mathbf{E}_{Coul}$) and reaction ($\mathbf{E}_{reac}$) components.
- Dielectric boundary, from the jump in ϵ across the molecular surface:

$$\mathbf{F}_{db} = -\int_\Omega \frac{1}{2}|\mathbf{E}|^2\nabla\epsilon\, d\mathbf{x} \tag{14}$$

- Ionic boundary (osmotic pressure), which appears as the ionic concentration drops to 0 inside the solute:

$$\mathbf{F}_{ib} = -\int_\Omega \frac{1}{2}\epsilon\kappa^2\phi^2\nabla\lambda\, d\mathbf{x} \tag{15}$$

  where λ is a mask function that is equal to 0 in Ω_1 and 1 in Ω_2.

Maxwell Stress Tensor Approach. Starting from the volume integral of the force density in eq 12, we can use the divergence theorem to write it in terms of a surface integral as

$$\mathbf{F} = \int_\Omega \mathbf{f}\, d\mathbf{x} = \int_\Omega \nabla\cdot\mathbf{P}\, d\mathbf{x} = \oint_\Gamma \mathbf{P}\cdot\mathbf{n}\, d\mathbf{x} \tag{16}$$

where $\mathbf{P}$ is a modified version of the Maxwell stress tensor that includes the effect of the salt concentration. Following the details in the work by Xiao et al.,[22] we obtain the following expression for the components of the stress tensor:

$$P_{ij} = \epsilon E_i E_j - \frac{1}{2}\epsilon E_k E_k \delta_{ij} - \frac{1}{2}\epsilon\kappa^2\phi^2\lambda\delta_{ij} \tag{17}$$

Different from the energy functional approach in eq 12, the Maxwell tensor does not distinguish the different sources of force. In the last term of eq 17 we find the ionic boundary

https://doi.org/10.1021/acs.jctc.3c00021
J. Chem. Theory Comput. 2023, 19, 2996−3006

force ($\mathbf{F}_{ib}$ in eq 15); however, $\mathbf{F}_q$ and $\mathbf{F}_{db}$ are mixed in the first two terms.

The $i, j \in \{1, 2, 3\}$ indices of the Maxwell stress tensor in eq 17 usually indicate the Cartesian x, y, and z components. However, it can be represented in any frame of reference. Following the work by Cai and co-workers,[33] we use a per-element local coordinate system ξ, η, τ, as shown in Figure 2,

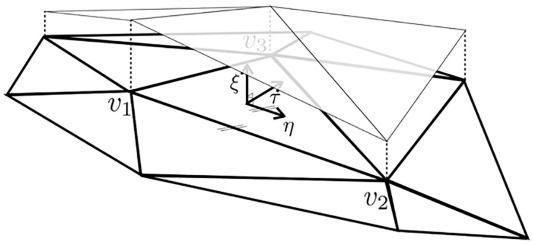

Figure 2. Local coordinate system for calculation of the force using the Maxwell stress tensor. Bottom set of triangles represents the surface mesh on the molecular surface, whereas the top set of triangles corresponds to the piecewise linear distribution of ϕ and $\partial\phi/\partial\mathbf{n}$.

centered at one vertex of the triangle. In this setting, ξ points in the direction normal to the panel, η points along one edge, and τ results from the cross product of the corresponding unit vectors ($\mathbf{e}_\tau = \mathbf{e}_\xi \times \mathbf{e}_\eta$). We can then write the normal vector in the integral of eq 16 as $\mathbf{n} = \mathbf{e}_\xi = (1, 0, 0)$, and applying the Maxwell tensor to it gives

$$\mathbf{P}\cdot\mathbf{n} = \left(\epsilon E_\xi E_\xi - \frac{1}{2}\epsilon|E|^2 - \frac{1}{2}\epsilon\kappa^2\phi^2\lambda\right)\mathbf{e}_\xi + \epsilon E_\xi E_\eta \mathbf{e}_\eta + \epsilon E_\xi E_\tau \mathbf{e}_\tau \tag{18}$$

which is the stress normal to the triangle. Evaluating eq 18 with the unit vectors $\mathbf{e}_\xi$, $\mathbf{e}_\eta$, and $\mathbf{e}_\tau$ expressed in Cartesian coordinates recasts the stress in the global frame of reference.

Numerical Method Implementation Details. *Numerical Solution of the Boundary Integral Equation.* We solve eq 5 numerically on a triangulation of the solvent-excluded surface using the `Bempp-cl` library.[34] `Bempp-cl` provides high-level abstractions of discretized forms of the single- and double-layer potentials (V and K) with an easy Python API, implemented in highly optimized OpenCL code for performance. This allows us to reach large-scale problems on a single workstation.

We assumed a continuous piecewise linear distribution of ϕ and $\partial\phi/\partial\mathbf{n}$ on the triangular panels. In that case, `Bempp-cl` tracks the values on the vertices of each triangle rather than the panel itself and uses a Galerkin approach to arrive at a linear system, such as

$$\begin{bmatrix} \frac{1}{2} + K^\Gamma_{\Gamma,L} & -V^\Gamma_{\Gamma,L} \\ \frac{1}{2} - K^\Gamma_{\Gamma,Y} & \frac{\epsilon_1}{\epsilon_2}V^\Gamma_{\Gamma,Y} \end{bmatrix} \begin{bmatrix} \phi \\ \frac{\partial\phi}{\partial\mathbf{n}} \end{bmatrix} = \begin{bmatrix} \frac{1}{\epsilon_1}\sum_k^{N_q} \frac{q_k}{4\pi|\mathbf{x}_\Gamma - \mathbf{x}_k|} \\ 0 \end{bmatrix} \tag{19}$$

Then the solution of this linear system yields the values of ϕ and $\partial\phi/\partial\mathbf{n}$ on the vertices, which we use on the discretized form of eq 10 to obtain ϕ_{reac} anywhere in the domain Ω_1.

Equation 19 is the matrix representation of eq 5, which is valid for the single-solute system in Figure 1. In practice, having just one solute is not an interesting setup to compute forces. The BEM formulation can consider more than one solute by applying the procedure that led to eq 5 over multiple surfaces,[11,35] which can define the molecular surface of another solute or a surface with imposed charge or potential.[15,36,37]

The Electric Field on the Molecular Surface with a First-Order Boundary Element Method. Solving the system in eq 19 using continuous piecewise linear elements with `Bempp-cl` gives ϕ and $\partial\phi/\partial\mathbf{n}$ on the triangle vertices. On the other hand, eq 18 needs the electric field $\mathbf{E} = -\nabla\phi$ in the normal (E_ξ) and tangential (E_η and E_τ) directions. Note that in the integration process to obtain the force, we consider E_ξ, E_η, and E_τ to be constant in each panel. The normal direction is easy to obtain, as it is an average of $-\partial\phi/\partial\mathbf{n}$ over the vertices of each triangle, which is appropriate even though the normal to the panel might be different from the normal to the vertex. However, the tangential directions require some work, and this is where the local coordinate system becomes useful. The numerical method assumes a linear distribution of ϕ on each

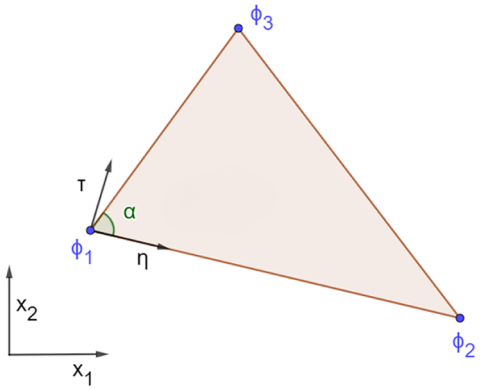

Figure 3. Local coordinate system for a triangular element.

panel, which lives on the (η, τ) plane (see Figure 3), allowing us to write

$$\phi(\eta, \tau) = a\eta + b\tau + c \tag{20}$$

Using Figure 3, we can determine a, b, and c from the values of ϕ on the three vertices (ϕ_1, ϕ_2, and ϕ_3), their relative distance (d_{12} and d_{13}), and the angle α at vertex 1. The local frame of reference is centered at vertex 1, and $\mathbf{e}_\eta$ points in the direction between vertices 1 and 2. Replacing on vertex 1 gives

$$\phi(0, 0) = a\cdot 0 + b\cdot 0 + c = \phi_1 \tag{21}$$

Then evaluating on $\eta = d_{12}$ gives

$$\phi(d_{12}, 0) = ad_{12} + b\cdot 0 + \phi_1 = \phi_2$$

$$a = \frac{\phi_2 - \phi_1}{d_{12}} \tag{22}$$

Finally, using the value at vertex 3 (ϕ_3) gives

$$\phi(d_{13}\cos(\alpha), d_{13}\sin(\alpha)) = \frac{\phi_2 - \phi_1}{d_{12}} d_{13}\cos(\alpha) + bd_{13}\sin(\alpha) + \phi_1 = \phi_3$$

$$b = \frac{\phi_3 - \phi_1}{d_{13}\sin(\alpha)} - \frac{\phi_2 - \phi_1}{d_{12}\tan(\alpha)} \tag{23}$$

https://doi.org/10.1021/acs.jctc.3c00021
J. Chem. Theory Comput. 2023, 19, 2996−3006

With the values of a, b, and c obtained from eqs 22, 23, and 21, we can compute the tangential field in each direction analytically as

$$E_\xi = -\frac{\partial \phi}{\partial \mathbf{n}}$$

$$E_\eta = -\frac{\partial \phi}{\partial \eta} = -\frac{\phi_2 - \phi_1}{d_{12}}$$

$$E_\tau = -\frac{\partial \phi}{\partial \tau} = -\frac{\phi_3 - \phi_1}{d_{13}\sin(\alpha)} + \frac{\phi_2 - \phi_1}{d_{12}\tan(\alpha)} \tag{24}$$

The computation of $\mathbf{E}$ with eq 24 does not introduce further approximations to the calculation. Then, in the context of a molecular surface represented with flat triangular panels and a piecewise linear variation of the potential and its normal derivative, the calculation of the field is exact. This stands out from other implementations of the force calculation with the Poisson−Boltzmann equation[4,5,12,31] that require numerical approximations on the molecular surface. For example, Lu and McCammon[31] used a similar approach with local coordinates on each panel but required an extra interpolation step to account for a piecewise constant node-patch scheme.

The Energy Functional Variation Approach in Boundary Integral Form. The Charge Force ($\mathbf{F}_q$). The charge force consists of an integration over the solute volume (see eq 13). Since the charge distribution (ρ_f) is a set of Dirac delta functions, the integral becomes a sum over the charges. Like the electrostatic potential leading to eq 10, the electric field can also be decomposed into reaction and Coulombic components ($\mathbf{E} = \mathbf{E}_{reac} + \mathbf{E}_{Coul}$). By the action−reaction principle, two point charges induce equal and opposite forces on them, canceling out the Coulomb contribution to the total force ($\int_\Omega \rho_f \mathbf{E}_{Coul}\, d\mathbf{x} = 0$). Then we can write

$$\mathbf{F}_q = \int_\Omega \rho_f \mathbf{E}_{reac}\, d\mathbf{x} = -\sum_i^N q_i \nabla \phi_{reac}(\mathbf{x}_i) \tag{25}$$

This could be computed by directly taking the derivative of eq 10, but the gradients of the potential operators V_Γ^x and K_Γ^x are currently not available in `Bempp-cl`. Thus, we calculated $\nabla\phi_{reac}(\mathbf{x}_i)$ by computing ϕ_{reac} at locations near each charge and used a centered difference scheme as

$$E_{i,reac}(\mathbf{x}_k) = -\frac{\partial \phi_{reac}}{\partial x_i} \approx -\frac{\phi_{reac}(\mathbf{x}_k + h_E\mathbf{e}_i) - \phi_{reac}(\mathbf{x}_k - h_E\mathbf{e}_i)}{2h_E} \tag{26}$$

where $i \in \{1, 2, 3\}$ indicates a Cartesian component and $\mathbf{x}_k$ is the position of charge k. We used $h_E = 0.001$ throughout this study, making sure that the mesh size of this finite difference approximation yielded an error that is low enough to not affect our results.

The Boundary Forces ($\mathbf{F}_{db}$ and $\mathbf{F}_{ib}$). The values of ϵ and λ have a sudden jump accross the molecular surface, making the gradients in eqs 14 and 15 difficult to compute with numerical methods. For example, finite difference codes like `APBS`[4,5] mollify the interface, making ϵ and λ vary across a few mesh points. The boundary integral formulation becomes convenient to avoid these inaccuracies.

Following the work by Cai and co-workers,[33] we can compute the force across the molecular surface due to the jump in dielectric constant by taking the difference of the terms with ϵ in the Maxwell stress tensor, evaluated on the inner (P_{ij}^{in}) and outer (P_{ij}^{out}) sides of Γ. In the local coordinate system from eq 18, this gives us the following force density:

$$\begin{aligned}\mathbf{f}_{db} &= (\mathbf{P}^{out} - \mathbf{P}^{in})\cdot\mathbf{n} = (\mathbf{P}^{out} - \mathbf{P}^{in})\cdot\mathbf{e}_\xi \\ &= \left\{\left[\left(\epsilon E_\xi E_\xi - \frac{1}{2}\epsilon|E|^2\right)\mathbf{e}_\xi + \epsilon E_\xi E_\eta \mathbf{e}_\eta + \epsilon E_\xi E_\tau \mathbf{e}_\tau\right]^{out}\right. \\ &\quad \left. - \left[\left(\epsilon E_\xi E_\xi - \frac{1}{2}\epsilon|E|^2\right)\mathbf{e}_\xi + \epsilon E_\xi E_\eta \mathbf{e}_\eta + \epsilon E_\xi E_\tau \mathbf{e}_\tau\right]^{in}\right\}\end{aligned} \tag{27}$$

Considering Ω_1 and Ω_2 the internal and external regions, respectively, we can apply the interface conditions

$$\begin{aligned}\epsilon_1 E_{1,\xi} &= \epsilon_2 E_{2,\xi} \\ E_{1,\eta} &= E_{2,\eta} \\ E_{1,\tau} &= E_{2,\tau}\end{aligned} \tag{28}$$

to cancel out the $\mathbf{e}_\eta$ and $\mathbf{e}_\tau$ components and write

$$\begin{aligned}\mathbf{f}_{db} &= \left[\left(\epsilon_2 E_{2,\xi}^2 - \frac{1}{2}\epsilon|E_2|^2\right) - \left(\epsilon_1 E_{1,\xi}^2 - \frac{1}{2}\epsilon|E_1|^2\right)\right]\mathbf{e}_\xi \\ &= \frac{1}{2}[\epsilon_2(E_{2,\xi}^2 - E_{2,\eta}^2 - E_{2,\tau}^2) - \epsilon_1(E_{1,\xi}^2 - E_{1,\eta}^2 - E_{1,\tau}^2)]\mathbf{e}_\xi \\ &= \frac{1}{2}[\epsilon_1 E_{1,\xi}E_{2,\xi} - \epsilon_2 E_{1,\xi}E_{2,\xi} - \epsilon_2(E_{2,\eta}E_{1,\eta} + E_{2,\tau}E_{1,\tau}) \\ &\quad + \epsilon_1(E_{2,\eta}E_{1,\eta} + E_{2,\tau}E_{1,\tau})]\mathbf{e}_\xi \\ &= \frac{1}{2}(\epsilon_1 - \epsilon_2)(E_{2,\xi}E_{1,\xi} + E_{2,\eta}E_{1,\eta} + E_{2,\tau}E_{1,\tau})\mathbf{e}_\xi \\ &= -\frac{1}{2}(\epsilon_2 - \epsilon_1)(\mathbf{E}_1\cdot\mathbf{E}_2)\mathbf{e}_\xi\end{aligned} \tag{29}$$

Equation 29 is in agreement with previous work from Davis and McCammon.[18] Then the total force $\mathbf{F}_{db}$ on the molecular surface is

$$\mathbf{F}_{db} = \oint_\Gamma \mathbf{f}_{db}\, d\mathbf{x} = -\frac{1}{2}(\epsilon_2 - \epsilon_1)\oint_\Gamma \mathbf{E}_1\cdot\mathbf{E}_2\mathbf{e}_\xi\, d\mathbf{x} \tag{30}$$

The electric fields $\mathbf{E}_1$ and $\mathbf{E}_2$ in eq 30 can be computed with eq 24. The tangential components of the field are usually much smaller than the normal one,[33] and $\mathbf{F}_{db}$ can be approximated as[15]

$$\mathbf{F}_{db}^{approx} = -\frac{1}{2}(\epsilon_2 - \epsilon_1)\frac{\epsilon_1}{\epsilon_2}\oint_\Gamma \left(\frac{\partial \phi_1}{\partial \mathbf{n}}\right)^2 \mathbf{n}\, d\mathbf{x} \tag{31}$$

This last expression is very convenient in a boundary integral framework, as $\partial\phi/\partial\mathbf{n}$ results directly from solving the system in eq 19, without limiting the choice of ansatz to piecewise linear.

To obtain a surface integral expression for the ionic pressure force ($\mathbf{F}_{ib}$), we can use the same approach that led to eq 30. This time, we compute the difference of the salt-related terms in the Maxwell stress tensor (λ in eq 17) on the inner and outer sides of Γ. This leads to

$$\mathbf{F}_{ib} = -\frac{1}{2}\kappa^2\epsilon_2\int_\Gamma \phi^2\mathbf{n}\, d\mathbf{x} \tag{32}$$

https://doi.org/10.1021/acs.jctc.3c00021
J. Chem. Theory Comput. 2023, 19, 2996−3006

RESULTS AND DISCUSSION

This section presents force calculations for isolated molecules and for two molecules interacting. We computed the force with the three approaches described in Methods, namely, the virtual displacement (eq 11), energy functional (eqs 25, 30, and 32), and Maxwell stress tensor (eqs 16 and 18) approaches. In the case of the energy functional approach, we also computed the dielectric boundary force with the normal approximation in eq 31 ($\mathbf{F}_{db}^{approx}$). This is summarized in Table 1, with a naming convention that is used in the rest of this section. To compare, we used the finite difference software APBS.[4,5]

Table 1. Summary and Naming Convention of Force Calculation Methods with BEM

Name	Description	Equation(s)	Reference
Method 1	Virtual displacement	11	18
Method 2	Energy functional variation	25, 30, and 32	16
Method 3	Approximated energy functional variation	25, 31, and 32	15
Method 4	Maxwell stress tensor integration	16 and 18	22

In all cases, the dielectric constant inside the protein was $\epsilon_1 = 4$, and the solvent was set to $\epsilon_2 = 80$ and $\kappa = 0.125$ Å^{-1} (corresponding to 150 mM monovalent ions in the solvent). We used the pdb2pqr[38] software to parametrize the atomic charges and radii and then Nanoshaper[39] to generate the surface mesh, unless otherwise noted. Both pdb2pqr and Nanoshaper are called from PBJ. Unless otherwise noted, we used a Gauss quadrature rule of order 4 and a GMRES tolerance of 10^{-5}.

The runs were performed on a workstation with two 12-core Intel Xeon E5-2680 v3 @ 2.5 GHz CPUs and 96 GB of RAM.

Results with a Single Molecule. As an initial test case, we ran experiments with the different methods detailed in Table 1 on a single lysozyme (PDB entry 1lyz), parametrized with the AMBER force field. As the protein is isolated, the total force should be zero, making this a good test case for accuracy. For the same reason, we did not run these experiments with Method 1.

Table 2 shows the solvation force and energy (eq 9) for Methods 2, 3, and 4 for different surface mesh refinements. As expected, all methods are converging to zero as the mesh density increases, but Method 4 generates the most accurate results and Method 3 the least. This is an expected result for two reasons. First, Method 3 behaves worse because it uses an approximation on the dielectric boundary force (eq 31) that neglects the electric field in off-normal directions. Second, Method 2 involves the sum of two large and opposite components, namely, $\mathbf{F}_q$ and $\mathbf{F}_{db}$ (see Table 3 for their magnitudes). This is a difficult situation for the numerical method, as small errors in $\mathbf{F}_q$ and $\mathbf{F}_{db}$ may result in a large error in their difference. This does not happen with Method 4. The force calculations with APBS in Table 4 also use the energy functional approach (similar to Method 2), and hence, they have the same accuracy issues. Even though the solution with APBS seems to be converging to zero, it performs worse than Method 2 and Method 3.

Table 2. Solvation Energy (in kcal/mol) and Force Magnitude (in kcal mol^{-1} Å^{-1}) for PDB Entry 1lyz at Different Mesh Densities (in Vertices/Å^2)

Mesh density	Method 2	Method 3	Method 4	ΔG_{solv}
2	5.2553	7.0078	0.6234	−484.70
4	2.0308	3.3422	0.2325	−465.74
8	0.8131	1.9724	0.1013	−458.31
16	0.3649	1.4639	0.0458	−455.22

Table 4. APBS Force Magnitude (in kcal mol^{-1} Å^{-1}) for PDB Entry 1lyz (Mesh Density in Δx Å, Box Size = 60 × 60 × 60)

Δx	Nodes	|F|
0.938	65 × 65 × 65	73.439
0.469	161 × 161 × 161	64.234
0.208	321 × 321 × 321	17.963
0.117	513 × 513 × 513	1.4699

To analyze the convergence, we can use the concept of *observed order of convergence* (p):[11,40]

$$p = \frac{\log\left(\frac{f_1 - f_2}{f_2 - f_3}\right)}{\log(r)} \tag{33}$$

where f_1, f_2, and f_3 are the solutions with a coarse, medium, and fine mesh, respectively, and r is the mesh density ratio between them. If the details of the solution are appropriately resolved, p should match the order of convergence of the numerical method, and we say it is in the *asymptotic convergent region*. Our boundary integral method uses linear elements that give first-order convergence. Considering the mesh densities 4, 8, and 16 vertices/Å^2 from Table 2 in eq 33, we get $p = 1.2$ for Method 4 and $p = 1.4$ for Method 2 and Method 3, which indicates that they all are asymptotically converging. Using the three finest meshes of APBS in Table 4 results in $p = 1.48$, which is similar to our BEM approach; however, the results are still far from the real solution ($|\mathbf{F}| = 0$). It is important to consider that force calculations with APBS use a fourth-order spline to mollify the dielectric interface and compute the electric field on the molecular surface, adding an extra layer of approximations.

Sørensen et al.[41] performed a careful analysis of the impact of mesh spacing on solvation and binding free energies for

Table 3. Force Decomposition (Magnitudes in kcal mol^{-1} Å^{-1}) for PDB Entry 1lyz Using Method 2 and Method 3 at Different Mesh Densities (in Vertices/Å^2)

	Method 2			Method 3		
Mesh density	$\lvert\mathbf{F}_q\rvert$	$\lvert\mathbf{F}_{db}\rvert$	$\lvert\mathbf{F}_{ib}\rvert$	$\lvert\mathbf{F}_q\rvert$	$\lvert\mathbf{F}_{db}\rvert$	$\lvert\mathbf{F}_{ib}\rvert$
2	38.0419	32.6898	0.1419	38.0419	30.9821	0.1419
4	29.2129	27.0556	0.1405	29.2129	25.7790	0.1405
8	27.6445	26.6999	0.1411	27.6445	25.5650	0.1411
16	26.2625	25.7651	0.1410	26.2625	24.6971	0.1410

https://doi.org/10.1021/acs.jctc.3c00021
J. Chem. Theory Comput. 2023, 19, 2996−3006

various finite difference codes (APBS among them). They recommended a spacing of $\Delta x = 0.5$ or less for acceptable binding energy results. On the other hand, a similar analysis with BEM[11] concludes that a mesh with 2 vertices/Å^2 is the coarsest refinement that yields acceptable results for solvation and binding energies. Table 4 shows that a mesh spacing of $\Delta x = 0.117$, which is 4× finer than Sørensen et al.'s recommendation, is less accurate than using 2 vertices/Å^2 with Method 4 and 8 vertices/Å^2 with Method 2. This indicates that a BEM approach with the same mesh that is valid for solvation energy calculations is useful to compute the force. This is not the case in finite differences, which has been reported in the past.[23]

Results for Two Spherical Molecules. Force calculations are useful to study the interaction between two or more molecules. As a simple model problem, we computed the force induced by a spherical molecule on another spherical molecule ($\mathbf{F}_{\text{bind}}$). In general, $\mathbf{F}_{\text{bind}}$ is the difference in force between an interacting state, where spheres are close by, and a noninteracting one. As there are only two spheres, the molecules are isolated in the noninteracting state, and the force is zero. For that reason, we only need to compute the force in the interacting state.

Both spheres had a centered charge of $2q_e$ and a radius of 1 Å, and we generated the meshes with MSMS.[42] In this case it makes sense to use Method 1 because the free energy depends on the relative distance between the spheres, which changes in the virtual displacement calculations (offset by $h\mathbf{e}_i$ with $h = 0.001$ Å) of eq 11. As the discretization error is small for a sphere, we refined other parameters to make sure that the convergence was not affected. In particular, we set the Gauss quadrature rule to order 8 and the GMRES tolerance to 10^{-8}.

Table 5 shows a mesh refinement study of the force and binding energy when the spheres are 3 Å away, where ΔG_{bind} is

Table 5. Solvation Force (x Component, in kcal mol^{-1} Å^{-1}) for Two Charges ($2q_e$ Each) in Spheres of 1 Å Radius Separated by 3 Å for Different Mesh Densities (in Vertices/Å^2)[a]

Mesh density	Method 1	Method 2	Method 3	Method 4	ΔG_{bind} (kcal/mol)
2	1.8794	1.9203	1.8944	1.8607	3.9338
4	1.9124	1.9374	1.8748	1.9062	3.9521
8	1.9268	1.9417	1.8652	1.9230	3.9611
16	1.9353	1.9429	1.8613	1.9346	3.9667
32	1.9390	1.9430	1.8599	1.9387	3.9689

[a]Using the virtual work approach with an analytical solution for the energy gives a force of 1.9425 kcal mol^{-1} Å^{-1}.

the energetic difference between interacting and isolated states. As a reference solution, we used closed expressions for the solvation energy of two spheres[43,44] and computed the force by applying them to the virtual displacement approach in eq 11. This reference value was $\mathbf{F}_{\text{ref}} = 1.9425$ kcal mol^{-1} Å^{-1}, which is the base in the error plots of Figure 4. It is interesting to note that even though Method 2 is more accurate than Method 4, the latter is converging with the expected first-order trend (as also Method 1) when Method 2 is not. Similarly to the isolated case with lysozyme, it is difficult to obtain the right convergence with Method 2, as it involves the subtraction of two large numbers ($\mathbf{F}_q$ and $\mathbf{F}_{\text{db}}$). This makes Method 4 a more robust option.

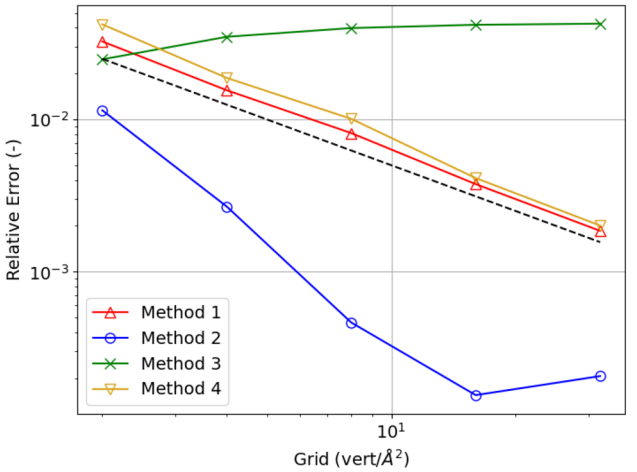

Figure 4. Error of each method for two 1 Å spheres with a centered $2q_e$ charge at a center-to-center distance of 3 Å. Dashed line indicates linear convergence.

Figure 5 shows the induced force at different center-to-center distances for the same two spheres, using an 8 vertices/

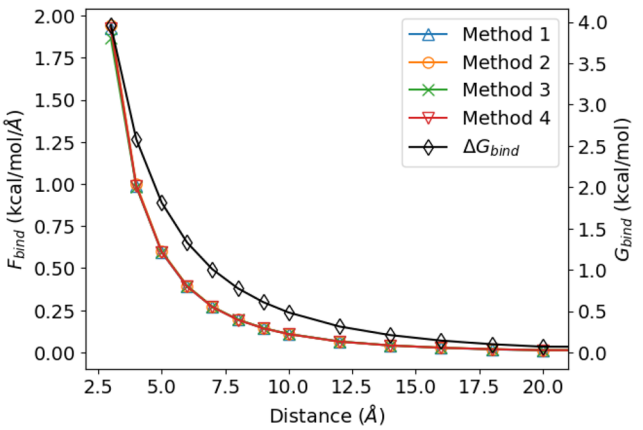

Figure 5. Induced force and binding energy between two spheres (each with radius 1 Å) with a centered $2q_e$ charge at different center-to-center distances.

Å^2 mesh and $h = 0.001$ Å for Method 1. Even though the errors in Figure 4 are different for Methods 2, 3, and 4, in the context of Figure 5 these curves are overlapped.

The fact that Method 2 does not converge linearly in Figure 4 is not surprising. This method involves the sum of large opposite values $\mathbf{F}_q$, $\mathbf{F}_{\text{db}}$, and $\mathbf{F}_{\text{ib}}$, yielding a smaller total force. Using a Richardson extrapolated value as an approximate exact solution for each component,[11,40] we performed a mesh convergence study (see Figure 6), which indicated linear convergence of $\mathbf{F}_q$, $\mathbf{F}_{\text{db}}$, and $\mathbf{F}_{\text{ib}}$ independently. Then, small errors that are not noticed in each component of the force have a large influence on the convergence of the total force of Figure 4.

Convergence of the Boundary Forces. The computation of the boundary forces is challenging, and results shown so far are not conclusive regarding its convergence. To further verify our implementation of $\mathbf{F}_{\text{db}}$ and $\mathbf{F}_{\text{ib}}$, we performed two variations to the test case in Table 5 and Figure 5:

https://doi.org/10.1021/acs.jctc.3c00021
J. Chem. Theory Comput. 2023, 19, 2996−3006

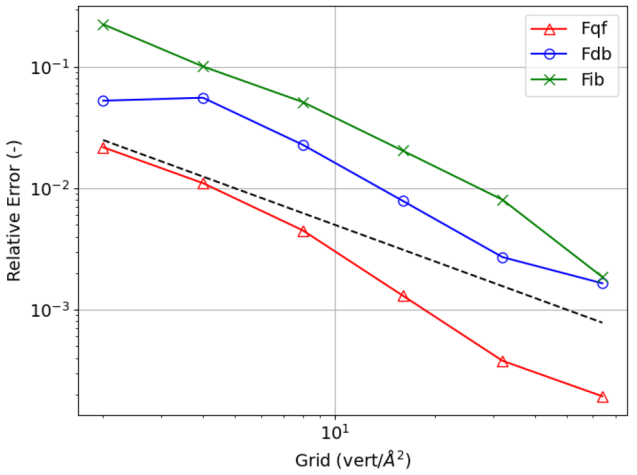

Figure 6. Error (with respect to an extrapolated value) of the different components of Method 2 for two 1 Å spheres with a centered $2q_e$ charge at 3 Å center-to-center distance. Dashed line indicates linear convergence.

1. We removed the charge from one sphere and set $\epsilon_2 = \epsilon_1 = 4$. Then there was no dielectric interface, and the computed force corresponded to the osmotic pressure ($\mathbf{F}_{ib}$) completely. A convergence analysis at a center-to-center distance of 3 Å is presented in Table 6, and Figure 7 shows its variation with distance using a 128 vertices/Å^2 mesh.

Table 6. Solvation Force (x Component, in kcal mol^{-1} Å^{-1}) for an Uncharged Spherical Cavity Interacting with a Sphere Containing a Single $2q_e$ Charge in a Low-Dielectric Solvent ($\epsilon_2 = 4$, $\kappa = 0.125$)[a]

Mesh density	Method 1	Method 2	Method 3	Method 4	ΔG_{bind} (kcal/mol)
2	−0.0304	−0.0331	−0.0331	−0.1286	0.0339
4	−0.0388	−0.0398	−0.0398	−0.0908	0.0419
8	−0.0419	−0.0423	−0.0423	−0.0732	0.0449
16	−0.0439	−0.0440	−0.0440	−0.0583	0.0469
32	−0.0447	−0.0448	−0.0448	−0.0520	0.0477
64	−0.0451	−0.0452	−0.0452	−0.0485	0.0481
128	−0.0453	−0.0453	−0.0453	−0.0470	0.0483
256	−0.0454	−0.0454	−0.0454	−0.0463	0.0484

[a]Both spheres have a 1 Å radius, and they are 3 Å apart (center-to-center). Mesh densities are in vertices/Å^2.

2. We removed the charge from one sphere and salt from the solvent ($\kappa = 0$). In this case, all the force on the neutral sphere corresponded to the dielectric boundary force ($\mathbf{F}_{db}$). A convergence analysis at a center-to-center distance of 3 Å is presented in Table 7, and Figure 8 shows its variation with distance using a 128 vertices/Å^2 mesh.

To ensure the appropriate accuracy, these runs used a GMRES tolerance of 10^{-8}. The results in Tables 6 and 7 show that all methods are converging to the same value and are indistinguishable in Figures 7 and 8. This verifies the implementation of $\mathbf{F}_{ib}$ and $\mathbf{F}_{db}$ in Method 2.

Using Method 1 as a reference, we can see from Table 6 that Methods 2 and 3 do a better job than Method 4 in computing the osmotic pressure $\mathbf{F}_{ib}$. This seems surprising, considering

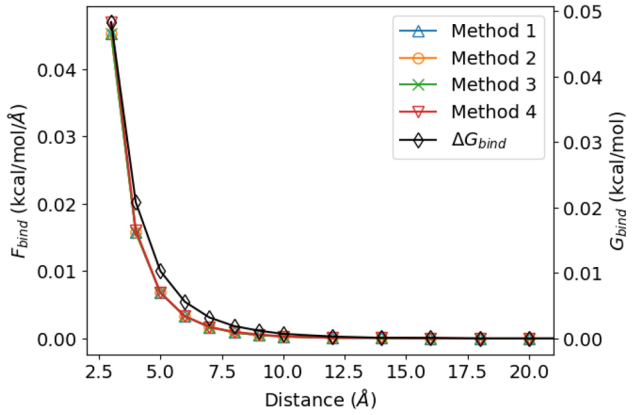

Figure 7. Induced force of a sphere with a $2q_e$ centered charge on another uncharged sphere and binding energy at different center-to-center distances. Both spheres had a radius of 1 Å, and the solvent dielectric was $\epsilon_2 = \epsilon_1 = 4$. The only source of this force is the osmotic pressure $\mathbf{F}_{ib}$.

Table 7. Solvation Force (x Component, in kcal mol^{-1} Å^{-1}) for an Uncharged Spherical Cavity Interacting with a Sphere Containing a Single $2q_e$ Charge in a Salt-Free Solvent ($\epsilon_2 = 80$, $\kappa = 0$)[a]

Mesh density	Method 1	Method 2	Method 3	Method 4	ΔG_{bind} (kcal/mol)
2	−0.0555	−0.0636	−0.0013	−0.0642	0.0391
4	−0.0689	−0.0729	−0.0020	−0.0733	0.0480
8	−0.0742	−0.0767	−0.0023	−0.0769	0.0514
16	−0.0776	−0.0789	−0.0025	−0.0790	0.0537
32	−0.0791	−0.0798	−0.0026	−0.0798	0.0546
64	−0.0798	−0.0802	−0.0026	−0.0802	0.0551
128	−0.0802	−0.0804	−0.0026	−0.0804	0.0554
256	−0.0804	−0.0805	−0.0027	−0.0805	0.0555

[a]Both spheres have a 1 Å radius, and they are 3 Å apart (center-to-center). Mesh densities are in vertices/Å^2.

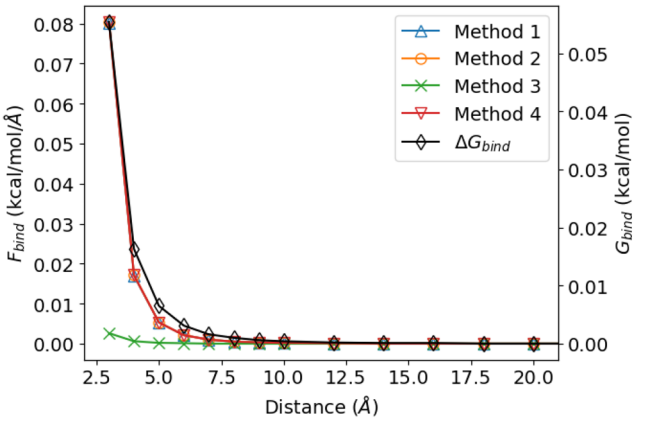

Figure 8. Induced force of a sphere with a $2q_e$ centered charge on another uncharged sphere and binding energy at different center-to-center distances. Both spheres had a radius of 1 Å, and the solvent had no salt ($\kappa = 0$). The only source of this force is the dielectric interface $\mathbf{F}_{db}$.

that Method 4 has been the most accurate consistently. However, $\mathbf{F}_{ib}$ is usually the smallest component of the force, limiting its contribution to the total error.

https://doi.org/10.1021/acs.jctc.3c00021
J. Chem. Theory Comput. 2023, 19, 2996−3006

As the results in Table 6 do not consider a dielectric interface, the normal field approximation from Method 3 has no effect, and methods 2 and 3 yield the exact same values. This is in contrast to Table 7, which is only due to the dielectric boundary and results with Method 3 are way off.

Results for the Barnase−Barstar Complex. The barnase−barstar complex is a standard case study for binding energy calculations.[12,45,46] Here we used chains B (barnase) and E (barstar) of the structure under PDB entry 1brs[47] and moved barstar up in the z direction, away from barnase. In the closest position, barstar was displaced 9 Å in the z direction (see Figures 9 and 10), which was the smallest displacement

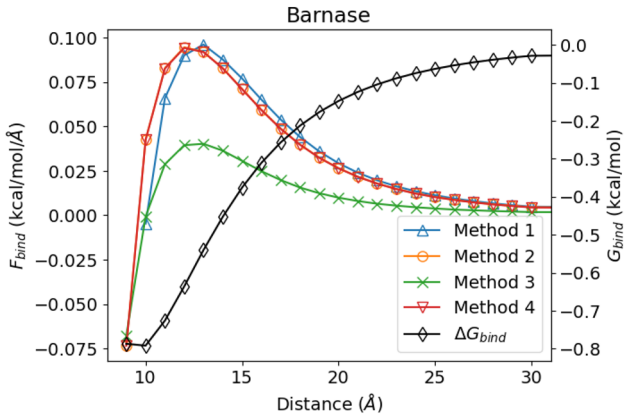

Figure 9. z component of force induced by barstar on barnase and binding energy at different offsets of barstar on the z axis with respect to its original position from the PDB crystal structure.

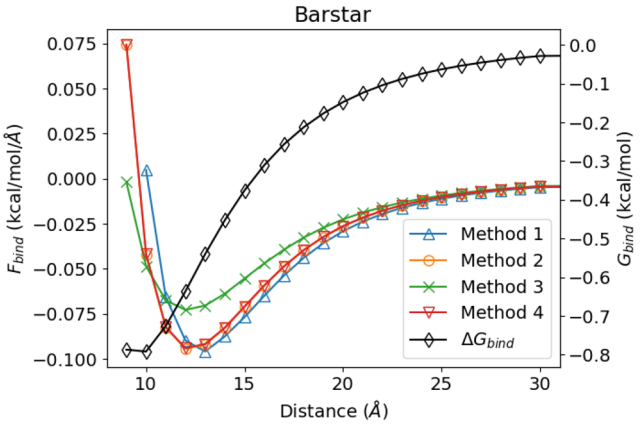

Figure 10. z component of force induced by barnase on barstar and binding energy at different offsets of barstar on the z axis with respect to its original position from the PDB crystal structure.

that did not generate clashes between the two molecular surfaces. We meshed the solvent-excluded surface of both molecules with 8 vertices/Å^2 and used h = 1 Å for Method 1.

Similar to the sphere case in Figure 5, the noninteracting state has both molecules isolated, where the force should be exactly zero, making the total force equal to $\mathbf{F}_{\text{bind}}$. However, from Table 2 we see that there is a numerical error, which decreases as the mesh is refined. To subtract out this error, we explicitly computed the force placing barstar and barnase far away (at 100 Å), and subtracted that out from the calculations performed at each distance.

Figures 9 and 10 show the z component of $\mathbf{F}_{\text{bind}}$ and ΔG_{bind} of barnase and barstar, respectively, as a function of the distance barstar was moved from its original position in the PDB structure. We can see that Method 2 and Method 4 overlap, whereas Method 3 performs worse. Even though for large distances the accuracy of Method 3 seems acceptable, as barnase and barstar get closer, the off-normal components of the field become more important, and the approximation in eq 31 is inadequate. Results with Method 1 are close to those with Methods 2 and 4. Computing the force with Method 1 for small distances is challenging because we need to avoid mesh clashing in the virtual displacements calculations of eq 11. Moreover, when the two molecules are close, ΔG_{bind} changes only slightly (see black curve for distances close to 10 Å in Figures 9 and 10), making it difficult to capture with the numerical derivative of eq 11. At large distances, all methods seem to perform similarly.

In our setup, barstar is placed above barnase on the z axis. Then, a positive z component of $\mathbf{F}_{\text{bind}}$ in Figure 9 indicates an attractive interaction, whereas attraction happens when the force is negative in Figure 10. As barstar approaches barnase, the interaction is initially attractive and then flips to repulsive. This is an indication that at small distances we would see a deceleration of the approaching molecules, in what is known as *soft landing*.[48]

CONCLUSIONS

The Poisson−Boltzmann equation is usually restricted to electrostatic potential and free energy calculations, but the force provides useful insights, for example, to study molecular interaction and binding, which can be tested experimentally.[49] As the force is a derivative of the energy, it is a challenging quantity to calculate numerically. Starting from piecewise linear boundary elements, our approach computes the electric field on the molecular surface exactly, without adding numerical approximations to the standard Poisson−Boltzmann calculation of the potential. Here we presented a thorough analysis of different formulations to obtain the force with a boundary element method. We compared four different methods and found that the most accurate one is based on the Maxwell stress tensor, followed by a method that relies on the variation of the energy functional. We also introduced an approximation to the energy functional approach that considers the normal component of the electric field only. This method gave acceptable results when the molecules were far apart. We verified our approach against known solutions for single molecules and two interacting spheres. We also compared the accuracy with that of the finite difference code and saw that the boundary integral approach outperforms the finite difference method for equivalent meshes.

In the future, we plan to use this efficient approach in applications where high accuracy is required for reliable simulations. Some examples are the force induced on large structures, such as viruses and materials,[15] and adsorption calculations,[50] where we need to detect the influence of small changes in orientation[36,51,52] on the total force.

ASSOCIATED CONTENT

Data Availability Statement

All the code and data required to reproduce the results of this work can be found in the repository at https://github.com/bem4solvation/paper_PBforces.

https://doi.org/10.1021/acs.jctc.3c00021
J. Chem. Theory Comput. 2023, 19, 2996−3006

AUTHOR INFORMATION

Corresponding Author

Christopher D. Cooper − *Department of Mechanical Engineering, Universidad Técnica Federico Santa María, 2390123 Valparaíso, Chile; Centro Científico Tecnológico de Valparaíso, Universidad Técnica Federico Santa María, 2390123 Valparaíso, Chile;* orcid.org/0000-0003-0282-8998; Email: christopher.cooper@usm.cl

Authors

Ian Addison-Smith − *Department of Mechanical Engineering, Universidad Técnica Federico Santa María, 2390123 Valparaíso, Chile*

Horacio V. Guzman − *Department of Theoretical Physics, Jožef Stefan Institute, 1000 Ljubljana, Slovenia; Departamento de Física Teórica de la Materia Condensada, Universidad Autónoma de Madrid, E-28049 Madrid, Spain;* orcid.org/0000-0003-2564-3005

Complete contact information is available at: https://pubs.acs.org/10.1021/acs.jctc.3c00021

Notes

The authors declare no competing financial interest.

ACKNOWLEDGMENTS

Financial support for this project was provided by Universidad Técnica Federico Santa María through Project PI-LIR-2020-10. C.D.C. acknowledges the support from CCTVal through ANID PIA/APOYO AFB220004. H.V.G. is thankful for the financial support by the Slovenian Research Agency (Funding No. P1-0055) and the financial support of the Community of Madrid and the European Union through the European Regional Development Fund (ERDF), financed as part of the Union response to COVID-19 pandemic.

REFERENCES

(1) Roux, B.; Simonson, T. Implicit solvent models. *Biophys. Chem.* **1999**, *78*, 1−20.

(2) Decherchi, S.; Masetti, M.; Vyalov, I.; Rocchia, W. Implicit solvent methods for free energy estimation. *Eur. J. Med. Chem.* **2015**, *91*, 27−42.

(3) Baker, N. A. Poisson−Boltzmann Methods for Biomolecular Electrostatics. *Methods Enzymol.* **2004**, *383*, 94−118.

(4) Baker, N. A.; Sept, D.; Joseph, S.; Holst, M. J.; McCammon, J. A. Electrostatics of nanosystems: application to microtubules and the ribosome. *Proc. Natl. Acad. Sci. U. S. A.* **2001**, *98*, 10037−10041.

(5) Jurrus, E.; Engel, D.; Star, K.; Monson, K.; Brandi, J.; Felberg, L. E.; Brookes, D. H.; Wilson, L.; Chen, J.; Liles, K.; Chun, M.; Li, P.; Gohara, D. W.; Dolinsky, T.; Konecny, R.; Koes, D. R.; Nielsen, J. E.; Head-Gordon, T.; Geng, W.; Krasny, R.; Wei, G.-W.; Holst, M. J.; McCammon, J. A.; Baker, N. A. Improvements to the APBS biomolecular solvation software suite. *Protein Sci.* **2018**, *27*, 112−128.

(6) Gilson, M. K.; Sharp, K. A.; Honig, B. H. Calculating the electrostatic potential of molecules in solution: method and error assessment. *J. Comput. Chem.* **1988**, *9*, 327−335.

(7) Bond, S. D.; Chaudhry, J. H.; Cyr, E. C.; Olson, L. N. A first-order system least-squares finite element method for the Poisson-Boltzmann equation. *J. Comput. Chem.* **2010**, *31*, 1625−1635.

(8) Boschitsch, A. H.; Fenley, M. O.; Zhou, H.-X. Fast boundary element method for the linear Poisson- Boltzmann equation. *J. Phys. Chem. B* **2002**, *106*, 2741−2754.

(9) Lu, B.; Zhang, D.; McCammon, J. A. Computation of electrostatic forces between solvated molecules determined by the Poisson−Boltzmann equation using a boundary element method. *J. Chem. Phys.* **2005**, *122*, 214102.

(10) Geng, W.; Krasny, R. A treecode-accelerated boundary integral Poisson−Boltzmann solver for electrostatics of solvated biomolecules. *J. Comput. Phys.* **2013**, *247*, 62−78.

(11) Cooper, C. D.; Bardhan, J. P.; Barba, L. A. A biomolecular electrostatics solver using Python, GPUs and boundary elements that can handle solvent-filled cavities and Stern layers. *Comput. Phys. Commun.* **2014**, *185*, 720−729.

(12) Li, L.; Chakravorty, A.; Alexov, E. DelPhiForce, a tool for electrostatic force calculations: Applications to macromolecular binding. *J. Comput. Chem.* **2017**, *38*, 584−593.

(13) Lu, B.; Cheng, X.; Huang, J.; McCammon, J. A. AFMPB: An adaptive fast multipole Poisson−Boltzmann solver for calculating electrostatics in biomolecular systems. *Comput. Phys. Commun.* **2013**, *184*, 2618−2619.

(14) Jha, A.; Nottoli, M.; Quan, C.; Stamm, B. Computation of forces arising from the linear Poisson−Boltzmann method in the domain-decomposition paradigm. *arXiv (Mathematics.Numerical Analysis)*, March 1, 2022, 2203.00552, ver. 1. https://arxiv.org/abs/2203.00552.

(15) Cooper, C. D.; Addison-Smith, I.; Guzman, H. V. Quantitative electrostatic force tomography for virus capsids in interaction with an approaching nanoscale probe. *Nanoscale* **2022**, *14*, 12232−12237.

(16) Gilson, M. K.; Davis, M. E.; Luty, B. A.; McCammon, J. A. Computation of electrostatic forces on solvated molecules using the Poisson-Boltzmann equation. *J. Phys. Chem.* **1993**, *97*, 3591−3600.

(17) Im, W.; Beglov, D.; Roux, B. Continuum solvation model: Computation of electrostatic forces from numerical solutions to the Poisson-Boltzmann equation. *Comput. Phys. Commun.* **1998**, *111*, 59−75.

(18) Davis, M. E.; McCammon, J. A. Calculating electrostatic forces from grid-calculated potentials. *J. Comput. Chem.* **1990**, *11*, 401−409.

(19) Lu, B.; Cheng, X.; Hou, T.; McCammon, J. A. Calculation of the Maxwell stress tensor and the Poisson-Boltzmann force on a solvated molecular surface using hypersingular boundary integrals. *J. Chem. Phys.* **2005**, *123*, 084904.

(20) Bordner, A. J.; Huber, G. A. Boundary element solution of the linear Poisson−Boltzmann equation and a multipole method for the rapid calculation of forces on macromolecules in solution. *J. Comput. Chem.* **2003**, *24*, 353−367.

(21) Lu, B.; Cheng, X.; Huang, J.; McCammon, J. A. An Adaptive Fast Multipole Boundary Element Method for Poisson- Boltzmann Electrostatics. *J. Chem. Theory Comput.* **2009**, *5*, 1692−1699.

(22) Xiao, L.; Cai, Q.; Ye, X.; Wang, J.; Luo, R. Electrostatic forces in the Poisson-Boltzmann systems. *J. Chem. Phys.* **2013**, *139*, 094106.

(23) Boschitsch, A. H.; Fenley, M. O. The Adaptive Cartesian Grid-Based Poisson−Boltzmann Solver: Energy and Surface Electrostatic Properties. In *Computational Electrostatics for Biological Applications*; Rocchia, W., Spagnuolo, M., Eds.; Springer, 2015; pp 73−110.

(24) Lu, B. Z.; Zhou, Y. C.; Holst, M. J.; McCammon, J. A. Recent Progress in Numerical Methods for the Poisson-Boltzmann Equation in Biophysical Applications. *Commun. Comput. Phys.* **2008**, *3*, 973−1009.

(25) Zauhar, R. J. The incorporation of hydration forces determined by continuum electrostatics into molecular mechanics simulations. *J. Comput. Chem.* **1991**, *12*, 575−583.

(26) Cortis, C. M.; Friesner, R. A. Numerical solution of the Poisson−Boltzmann equation using tetrahedral finite-element meshes. *J. Comput. Chem.* **1997**, *18*, 1591−1608.

(27) Search, S. D.; Cooper, C. D.; van't Wout, E. Towards optimal boundary integral formulations of the Poisson−Boltzmann equation for molecular electrostatics. *J. Comput. Chem.* **2022**, *43*, 674−691.

(28) Connolly, M. L. Analytical Molecular Surface Calculation. *J. Appl. Crystallogr.* **1983**, *16*, 548−558.

(29) Yoon, B. J.; Lenhoff, A. M. A boundary element method for molecular electrostatics with electrolyte effects. *J. Comput. Chem.* **1990**, *11*, 1080−1086.

(30) Juffer, A.; Botta, E. F.; van Keulen, B. A.; van der Ploeg, A.; Berendsen, H. J. The electric potential of a macromolecule in a

solvent: A fundamental approach. *J. Comput. Phys.* **1991**, *97*, 144−171.
(31) Lu, B.; McCammon, J. A. Improved Boundary Element Methods for Poisson-Boltzmann Electrostatic Potential and Force Calculations. *J. Chem. Theory Comput.* **2007**, *3*, 1134−1142. PMID: 26627432.
(32) Che, J.; Dzubiella, J.; Li, B.; McCammon, J. A. Electrostatic free energy and its variations in implicit solvent models. *J. Phys. Chem. B* **2008**, *112*, 3058−3069.
(33) Cai, Q.; Ye, X.; Luo, R. Dielectric pressure in continuum electrostatic solvation of biomolecules. *Phys. Chem. Chem. Phys.* **2012**, *14*, 15917−15925.
(34) Betcke, T.; Scroggs, M. Bempp-cl: A fast Python based just-in-time compiling boundary element library. *J. Open Source Software* **2021**, *6*, 2879−2879.
(35) Altman, M. D.; Bardhan, J. P.; White, J. K.; Tidor, B. Accurate solution of multi-region continuum biomolecule electrostatic problems using the linearized Poisson−Boltzmann equation with curved boundary elements. *J. Comput. Chem.* **2009**, *30*, 132−153.
(36) Cooper, C. D.; Clementi, N. C.; Barba, L. A. Probing protein orientation near charged nanosurfaces for simulation-assisted biosensor design. *J. Chem. Phys.* **2015**, *143*, 124709. Preprint on arxiv:1503.08150.
(37) Cooper, C. D.; Barba, L. A. Poisson−Boltzmann model for protein−surface electrostatic interactions and grid-convergence study using the PyGBe code. *Comput. Phys. Commun.* **2016**, *202*, 23−32.
(38) Dolinsky, T. J.; Nielsen, J. E.; McCammon, J. A.; Baker, N. A. PDB2PQR: an automated pipeline for the setup of Poisson−Boltzmann electrostatics calculations. *Nucleic Acids Res.* **2004**, *32*, W665−W667.
(39) Decherchi, S.; Rocchia, W. A general and robust ray-casting-based algorithm for triangulating surfaces at the nanoscale. *PLoS One* **2013**, *8*, No. e59744.
(40) Roache, P. J. *Verification and Validation in Computational Science and Engineering*; Hermosa Publishers: Albuquerque, NM, 1998.
(41) Sørensen, J.; Fenley, M. O.; Amaro, R. E. A Comprehensive Exploration of Physical and Numerical Parameters in the Poisson−Boltzmann Equation for Applications to Receptor−Ligand Binding. In *Computational Electrostatics for Biological Applications*; Rocchia, W., Spagnuolo, M., Eds.; Springer, 2015; pp 39−71.
(42) Sanner, M.; Olson, A. J.; Spehner, J. C. Reduced Surface: An Efficient Way to Compute Molecular Surfaces. *Biopolymers* **1996**, *38*, 305−320.
(43) Lotan, I.; Head-Gordon, T. An analytical electrostatic model for salt screened interactions between multiple proteins. *J. Chem. Theory Comput.* **2006**, *2*, 541−555.
(44) Siryk, S. V.; Bendandi, A.; Diaspro, A.; Rocchia, W. Charged dielectric spheres interacting in electrolytic solution: A linearized Poisson−Boltzmann equation model. *J. Chem. Phys.* **2021**, *155*, 114114.
(45) Bertonati, C.; Honig, B.; Alexov, E. Poisson-Boltzmann calculations of nonspecific salt effects on protein-protein binding free energies. *Biophys. J.* **2007**, *92*, 1891−1899.
(46) Nguyen, D. D.; Wang, B.; Wei, G.-W. Accurate, robust, and reliable calculations of Poisson−Boltzmann binding energies. *J. Comput. Chem.* **2017**, *38*, 941−948.
(47) Buckle, A. M.; Schreiber, G.; Fersht, A. R. Protein-protein recognition: Crystal structural analysis of a barnase−barstar complex at 2.0 Å resolution. *Biochemistry* **1994**, *33*, 8878−8889.
(48) Shashikala, H. B. M.; Chakravorty, A.; Alexov, E. Modeling Electrostatic Force in Protein-Protein Recognition. *Front. Mol. Biosci.* **2019**, *6*, 94.
(49) Hernando-Pérez, M.; Cartagena-Rivera, A.; Lošdorfer Božič, A.; Carrillo, P. J.; San Martín, C.; Mateu, M. G.; Raman, A.; Podgornik, R.; De Pablo, P. Quantitative nanoscale electrostatics of viruses. *Nanoscale* **2015**, *7*, 17289−17298.
(50) Staniscia, F.; Guzman, H. V.; Kanduc, M. Tuning contact angles of aqueous droplets on hydrophilic and hydrophobic surfaces by surfactants. *J. Phys. Chem. B* **2022**, *126*, 3374−3384.
(51) Tsori, Y. Bistable colloidal orientation in polar liquid near a charged wall. *J. Colloid Interface Sci.* **2020**, *559*, 45−50.
(52) Urzúa, S. A.; Sauceda-Oloño, P. Y.; García, C. D.; Cooper, C. D. Predicting the orientation of adsorbed proteins steered with electric fields using a simple electrostatic model. *J. Phys. Chem. B* **2022**, *126*, 5231−5240.

https://doi.org/10.1021/acs.jctc.3c00021
J. Chem. Theory Comput. 2023, 19, 2996−3006